Chem Soc Rev

3D-printing technologies for electrochemical applications

Journal:	*Chemical Society Reviews*
Manuscript ID	CS-SYN-09-2015-000714.R3
Article Type:	Tutorial Review
Date Submitted by the Author:	08-Mar-2016
Complete List of Authors:	Ambrosi, Adriano; Nanyang Technological University, Chemistry and Biological Chemistry Pumera, Martin; Nanyang Technological University, Chemistry and Biological Chemistry

Tutorial review

3D-printing technologies for electrochemical applications

Adriano Ambrosi* and Martin Pumera*

Division of Chemistry & Biological Chemistry, School of Physical and Mathematical Sciences, Nanyang Technological University, Singapore 637371, Singapore.

*Correspondence to be addressed to: M. Pumera, pumera.research@gmail.com; A. Ambrosi, ambrosi@ntu.edu.sg

Abstract

Since its conception during the eighties, 3D printing, also known as additive manufacturing, has been receiving unprecedented levels of attention and interest from industry and research laboratories. This is in addition to end users, who have benefited from the pervasiveness of desktop-size and relatively cheap printing machines available. 3D printing enables almost infinite possibilities for rapid prototyping. Therefore, it has been considered for applications in numerous research fields, ranging from mechanical engineering, medicine, and materials science to chemistry. Electrochemistry is another branch of science that can certainly benefit from 3D-printing technologies, paving the way for the design and fabrication of cheaper, higher performing, and ubiquitously available electrochemical devices. Here, we aim to provide a general overview of the most commonly available 3D-printing methods along with a review of recent electrochemistry related works adopting 3D printing as a possible rapid prototyping fabrication tool.

Keywords: 3D printing, electrochemistry, additive manufacturing, sensing, capacitance

TOC

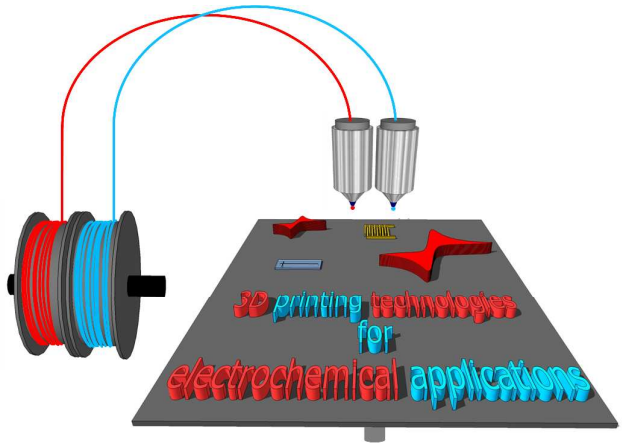

Key learning points

- Process of additive manufacturing (3D printing)
- Basics of 3D-printing technologies currently available
- Up-to-date usage of 3D printing for electrochemical applications

Content

1. Introduction

3D printing can be defined as a process used to fabricate three dimensional objects based on the digitally controlled deposition of successive layers of material until a final structure is created.[1] Also known as *additive manufacturing*, 3D printing follows the opposite fabrication principles of *subtractive manufacturing* where three-dimensional objects are created using material-removal processes such as drilling, milling, sawing, broaching, etc.[2] For rapid prototyping, both additive and subtractive manufacturing are valid methodologies. The choice depends on consideration of some factors such as the complexity of the objects to be created, the material employed, the number of replicates needed, and, of course, the cost. The geometrical complexity of the object represents the factor that primarily differentiates the two methods. Complex designs with several hollow parts can only be obtained by additive manufacturing since these parts are printed together with the solid portions in a layer-by-layer fashion. For simpler designs, the type of material plays an important part. Additive manufacturing is generally used to produce plastic-based objects, while subtractive manufacturing is the method of choice for most metal- as well as wooden-based objects. Subtractive manufacturing might be convenient if numerous replicates of the same part have to be produced in a shorter time, which also factors in on the production cost. Beside these differences, it is important to consider that additive manufacturing could greatly reduce energy costs by making use of less energy-demanding machines and also significantly reduce material waste (Figure 1).

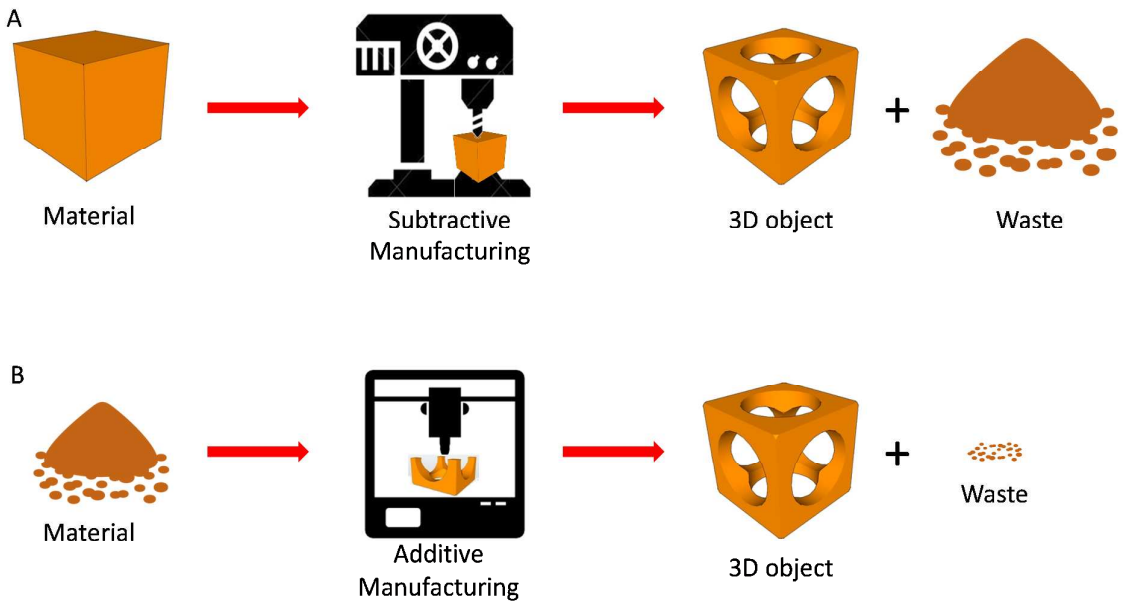

Figure 1. Additive *vs.* subtractive manufacturing. **A**) In subtractive manufacturing, a block of material is processed by material-removing machines according to digital design before obtaining the final 3D object together with a large amount of residual material. **B**) In additive manufacturing, a starting material (powder, liquid, filament, etc.) is processed by a 3D-printing machine, which deposits just the required amount of material in layer-by-layer fashion before the final 3D object is obtained. The amount of residual material left over after the process is significantly lower than that resulting from subtractive manufacturing.

2. 3D-printing process and techniques

The process of 3D printing starts with the creation of a virtual model of the object to be printed. This can be achieved by using computer-aided design (CAD) software, a three-dimensional scanner, or by means of photogrammetry where the model is obtained through the combination of several images of the object taken from different positions. Once the 3D model is created, it needs to be converted to the .STL file format (from STereoLithography), which stores the information of the model's surfaces as a list of coordinates of triangulated

sections. This file format is universally recognized as it can be read by all 3D printer software, which then converts the data to a G-code file after a "slicing" process. The slicing procedure consists of the generation of several 2D cross section layers of the entire object. Finally, the printer starts depositing the material following the successive sequencing of such 2D layers, which are built one on top of the other, until a 3D object is created (Figure 2).[3] Several 3D-printing technologies have been invented, each with methodology differing in the way the 2D layers of material are deposited. These can be grouped into four main categories based on their respective common mechanism/principle: 1) photopolymerization; 2) extrusion; 3) powder based; and 4) lamination.

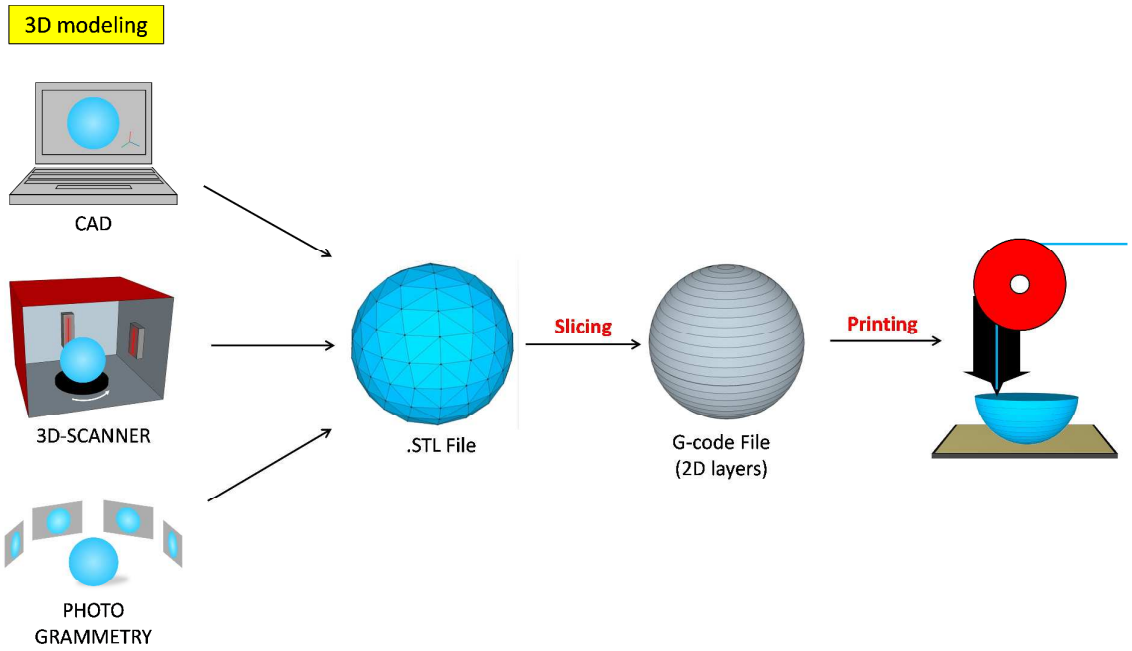

Figure 2. 3D-printing process. A digital model of the object is obtained through CAD software, a 3D scanner, or a photogrammetry procedure. The 3D model design is then converted to the .stl format. A slicing process is then applied by the printer software to convert the .stl file data into a G-code file containing geometrical information of a series of 2D layers in which the model is divided. Finally, the printer starts depositing the material following the layer-by-layer sequence dictated by the G-code file.

2.1 Photopolymerization

Photopolymerization is one of the first employed mechanisms for 3D printing. The technique itself was invented during the 1980s. In 1981, Hideo Kodama devised a method to build three-dimensional objects by curing a photo-hardening polymer with UV light. The liquid polymer is solidified at its surface by exposure to UV light. Immersing this solidified layer in a controlled way enables successive layers to be solidified and stacked one on top of each other with good adhesion until a final 3D object is created.[4] In 1984, Charles Hull developed the first commercial system based on this method. Since then, the method has been known as stereolithography (SLA). He also founded the company 3D Systems, Corp.[5] Besides the commercialization of the first 3D printer, Hull also invented and introduced the .STL file format to link digital design with 3D-printing systems. The .STL format is still widely used. The UV curing system can either consist of a laser, which moves across the polymer surface according to the layer design (direct laser writing), or can make use of a digital mirror device (digital light projection), which projects UV light once for each layer according to the design. As for the polymerization process, this can either occur at the liquid surface (bath configuration), with the stage moving downwards after each layer is solidified (Figure 3A), or it can be obtained from the bottom, using an optically transparent window with the stage moving upwards upon layer formation (layer configuration or bat configuration, Figure 3B). This second approach is useful when the resin polymer is only available in limited quantities, where a lower volume will suffice.

Based on the same principle of photopolymerization, polyjet technology uses inkjet methods to deposit photocurable material at an exact position as dictated by the layer design, followed immediately by full area UV light illumination, which hardens the layer. For complex designs, a support material is also deposited to facilitate the freestanding of the printed structure. This technology, invented at Stratasys, enables much higher resolution (Figure 3C).

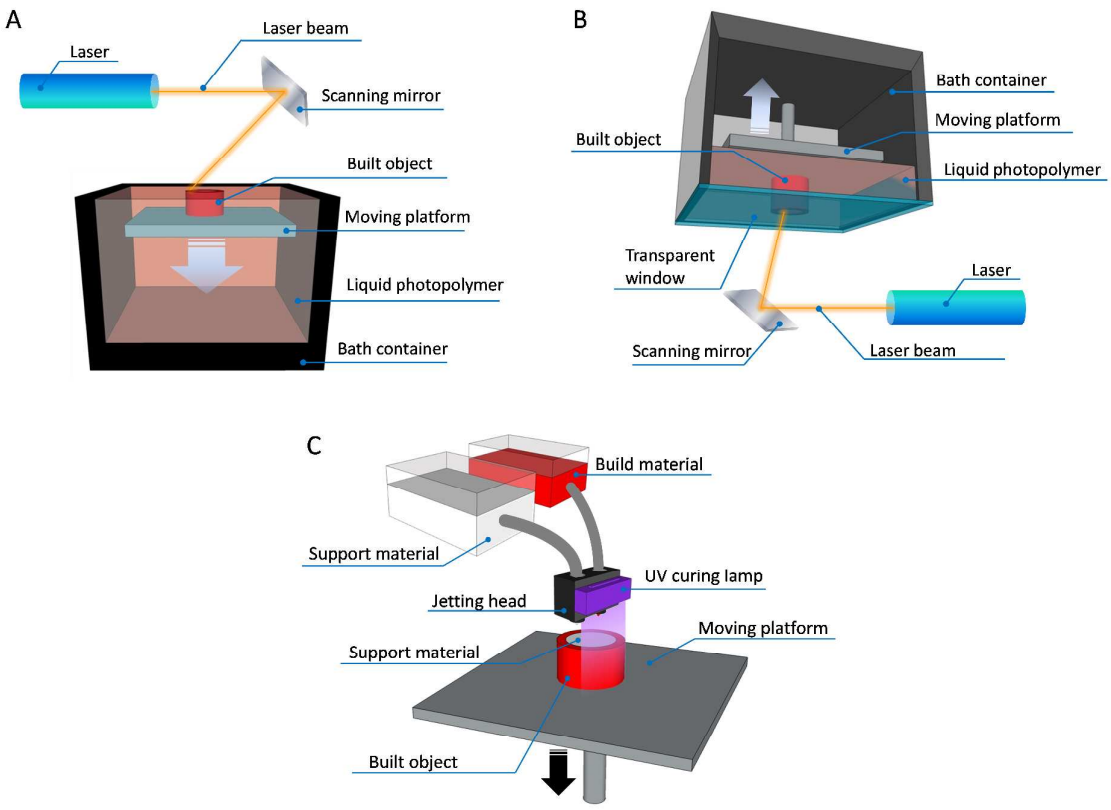

Figure 3. 3D-printing methods based on photopolymerization. **A**) Stereolithography (SLA) in a bath configuration where a laser beam is scanned across the liquid surface to polymerize the resin. Successive layers are created by lowering the movable table, allowing fresh liquid resin to be exposed. **B**) SLA in a layer configuration in which a laser beam is scanned from the bottom of the liquid tank through a transparent window. The polymerized layer attaches to the table, which is then moved upwards to refill the gap between the first layer and the window with fresh resin. **C**) Material jetting technology by which photocurable material is ink-jetted on the build tray together with the supporting material. A UV light then scans the layer's surface to harden the material. Once the layer is formed, the table is moved downwards and the next layer of material is ink-jetted and hardened.

2.2 Extrusion

Extrusion-based 3D-printing methods generally consist of the deposition of model material (and/or support material) directly from a nozzle head dispenser after material pretreatment such as liquefaction. The most common 3D technology employing this method is known as

fused deposition modeling (FDM), which creates 3D objects using thermoplastic materials. Invented by Scott Crump in 1989,[6] fused deposition modeling produces 3D objects by depositing, in a layer-by-layer manner, thermoplastic materials that were heated to their semi-molten state before extrusion at the dispenser nozzle. Once deposited, the material solidifies creating a uniform hard layer which stacks on top of the previous layer according to the sliced model design. Today, this method represents the most common 3D-printing technology due to its simplicity and the availability of machines at affordable prices. Thermoplastic materials such as polylactic acid (PLA), acrylonitrile butadiene styrene (ABS), polycarbonate (PC), polyamide (PA), etc. are usually employed and provided in filament form (as feeding spools) (Figure 4A). Different nozzles with varying materials can be employed simultaneously during a single printing process, creating multi-material structures. Materials can also be used as a supporting or sacrificial structure that will later be removed from the finished object. Using a very similar principle, robocasting (or direct ink writing) technology allows the controlled deposition of a much larger variety of materials or a combination of materials provided that they are in "ink" form, that is, in a highly viscous liquid state, which are able to retain their shape after deposition. This 3D-printing technology is extremely versatile since an almost infinite number of materials can be deposited, ranging from ceramic, plastics, and food to living cells (Figure 4B).[7,8] The type of material, viscosity and density of the ink, as well as the particle size within, dictates the type of dispenser to be used. The nozzle size and other specific requirements can also be adjusted to obtain optimal deposition. Even though the created object is usually freestanding, a post-fabrication process may be necessary to harden it and improve its mechanical properties via steps of drying, heating, or sintering.

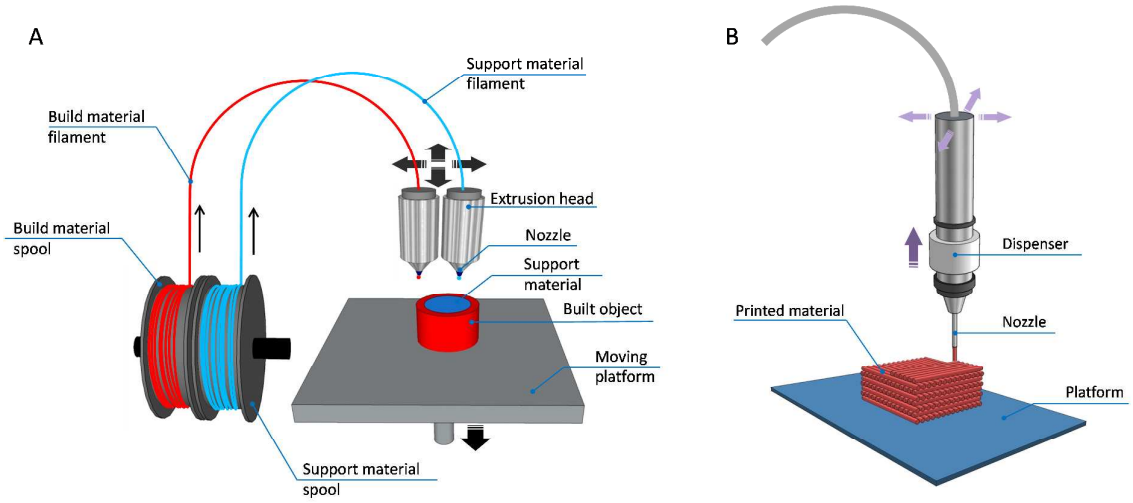

Figure 4. **A**) Schematic diagram of fused deposition modeling (FDM). A nozzle fed with a thermoplastic wire is moved in three dimensions across the building platform onto which molten voxels of polymer are applied. **B**) Schematic diagram of robocasting (direct ink writing). A material dispenser connected to a computer-controlled robot, scans across the building platform, depositing the ink material in a layer-by-layer manner.

2.3 Powder based

This method of additive manufacturing is based on the use of solid materials as building blocks, using particulates (particle size between 50-100 μm), for the 3D object. Conceptually, the printing process is similar to SLA, with the liquid photopolymer being replaced by powder, which is later distributed onto the building stage as thin layers through rollers or squeegees. At this point, a binding system (liquid glue, laser beams, etc.) is directed onto the powder layer, linking the particles at exact positions according to the cross-sectional model design. Once the solid layer has been formed, the stage is lowered to allow distribution of a second layer of powder on top of the first one, in preparation for the next binding process. In principle, a large variety of materials can be employed given that small particulate forms of plaster, ceramic, acrylic, wood, marble, and metal powders are readily available. An

important advantage of this technology is that the remaining non-bonded powder can function as a support material during the printing process. Therefore, no extra material is required to be co-printed. In addition, once the process is completed, all excess powder can be recovered and reused for another printing job, resulting in a great reduction of material waste.

The easiest binding system utilizes a traditional inkjet printing dispenser to precisely deposit liquid glue (or any chemical binder) inks onto the powder bed, according to the model design. This printing technology is known as binder jetting (Figure 5A). Alternatively, it is possible to bind the powder particles using high-energy laser beams, which sinter the particles just below the melting point (selective laser sintering, SLS) or reach melting temperatures to fuse the particles together (selective laser melting, SLM) (Figure 5B). These laser beam binding systems are mostly used for metal and alloy particles such as steel, pure titanium, aluminum, nickel, titanium, and bronze or precious-metal-based alloys, etc. More recently, it has been proposed that the use of electron beams to achieve higher temperatures endows improved mechanical properties to the metallic object being created (electron beam melting, EBM).[9, 10]

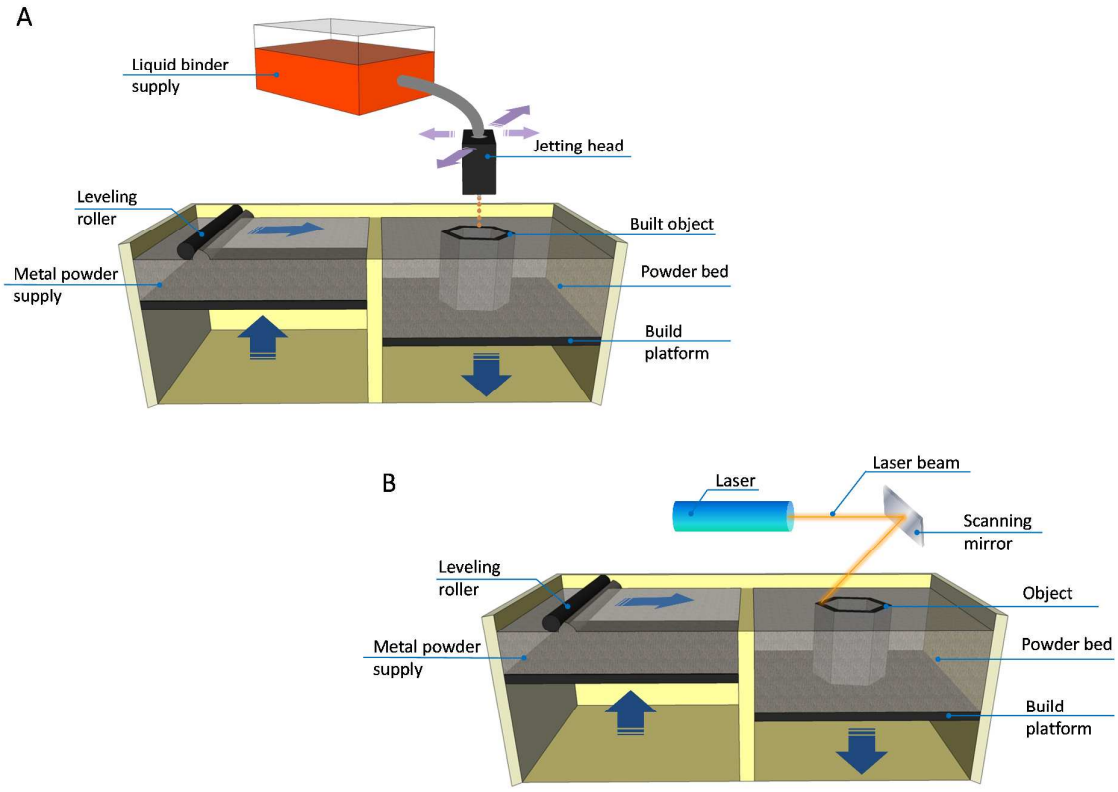

Figure 5. **A**) Schematic diagram of binder jetting 3D printing. A powder supply combined with a leveling roller distributes a thin layer of powder material onto the building platform. An inkjet dispenser controlled by a computer deposits the glue (or binder) liquid according to the layer design. Once the layer is completed, a second layer of powder is distributed onto the preceding one by the controlled upward movement of the supply container and downward movement of the building platform. **B**) Schematic diagram of laser beam sintering (SLS) (or melting, SLM). In this case, instead of the liquid binder being deposited by inkjet printing, a laser beam is used to sinter or fuse the particles locally according to the layer design.

2.4 Lamination

The process of lamination 3D printing involves the stacking of laminated material (components available in sheets) on top of one another after a layer contour definition was achieved by cutting tools. This technology, also known as laminated object manufacturing (LOM), was invented at Helisys during the late 1980s.[11] First, a sheet of material is loaded onto a stage and then undergoes a laser (or blade) cutting process, defining a cross-sectional

contour of the layer in accordance with a specific CAD design. Once the excess material is removed, a second sheet is loaded on top of the first one and again traced. Depending on the type of material, which could be paper, metal, plastic, etc., each layer is bonded to the preceding one using adhesives or welding techniques. The process is repeated many times until the 3D object is finally created (Figure 6).

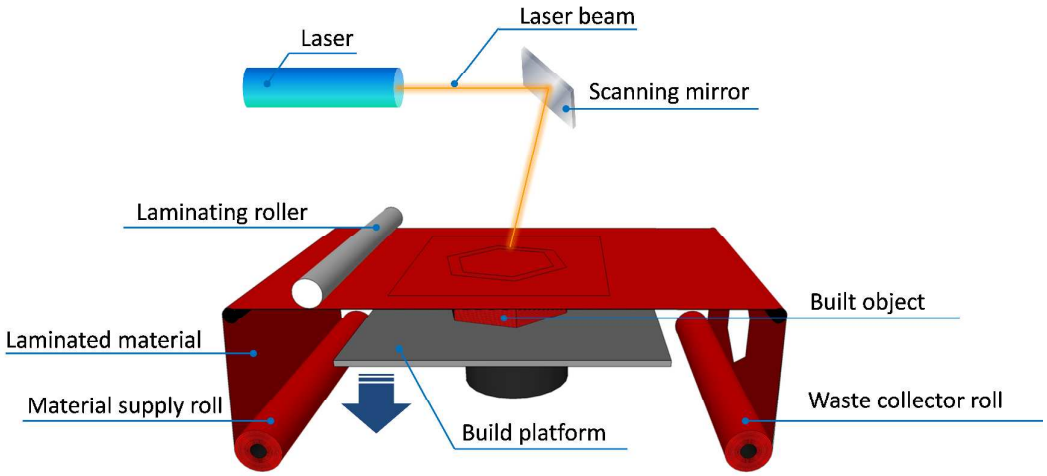

Figure 6. Schematic diagram of laminated object manufacturing (LOM). A first sheet of material is loaded onto the building platform. A PC-controlled cutting system consisting of a laser beam or a mechanical blade is then used to define the layer contour. Once the excess material is removed, a new sheet is loaded with a laminating roller which ensures good adhesion of the layers.

2.5 Recent developments: new materials, methods, and concepts

3D-printing technologies will certainly continue to evolve, thanks to numerous research labs attempting to implement new concepts, to fabricate faster, cheaper, and smaller printing systems, to increase printing definition, and to fabricate objects using materials that once could only be processed by subtractive manufacturing. In general, 3D-printing advancements are mainly aimed in three possible directions: i) developing printing systems that are able to print new materials; ii) increasing printing speed by means of new deposition concepts; and

iii) reaching micro-nanoscale resolution. Here, we wish to illustrate some examples from recent developments in 3D printing where either a new material or innovative printing process has been implemented.

Based on the principle of extrusion and bearing a similarity to the fused deposition modeling (FDM) technique, a research team at MIT very recently demonstrated a fully functional material extrusion printer for optically transparent glass. A special heating head and nozzle are able to liquefy glass for controlled spatial deposition according to CAD designs (Figure 7).[12] This method enables the fabrication of real glass objects with features and characteristics similar to traditionally produced glass articles. The method differs from the binder jetting method or sintering process of glass particles, which produces extremely fragile objects that have properties dissimilar to those of glass.

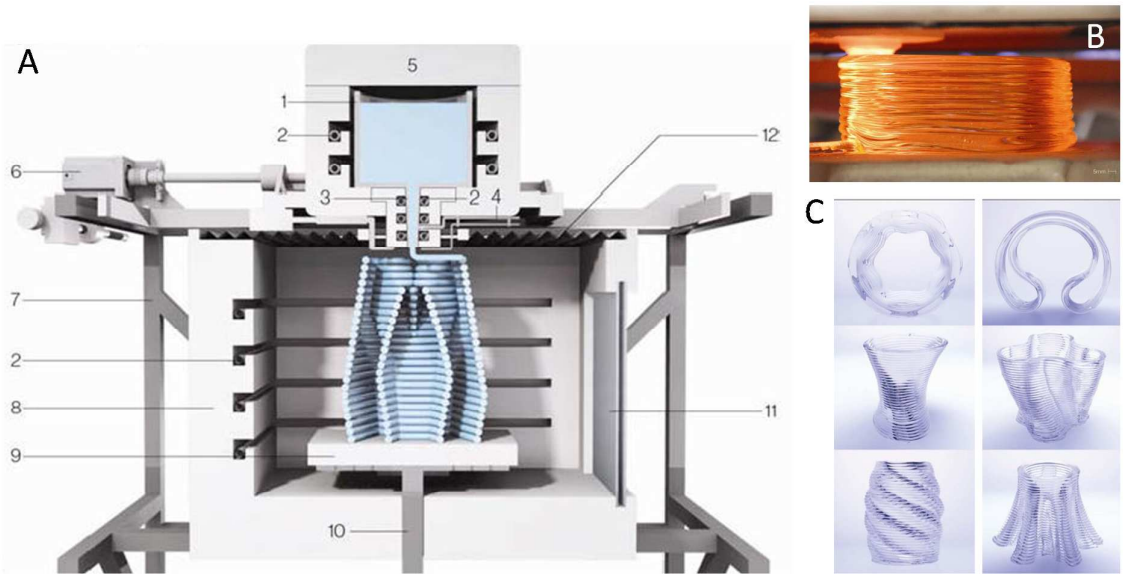

Figure 7. **A**) Rendered cross section of system showing the printer during fabrication. Detailed elements are: (1) crucible, (2) heating elements, (3) nozzle and (4) thermocouple, (5) removable feed access lid, (6) stepper motors, (7) printer frame, (8) print annealer, (9) ceramic print plate, (10) z-drive train, (11) ceramic viewing window, and (12) insulating skirt. **B**) Evolution of the printing process. **C**) Objects printed using the platform with various geometrical parameters. Adapted with permission from ref [12]. Copyright (2015) Mary Ann Liebert, Inc.

Additive manufacturing of metal parts generally relies on sintering (or melting) powder bed metal particles. A novel extrusion-based approach has recently been proposed to print 3D metal objects using a metal wire feed system.[13] This process is similar to FDM and requires a heating system to locally melt solid metal wire, creating a sort of pool of molten metal. Depending on the energy source, three technologies have recently emerged: electron beam freeform fabrication (Figure 8A),[14] wire-laser (Figure 8B)[15] and wire-arc-welding additive manufacturing (Figure 8C).[16, 17]

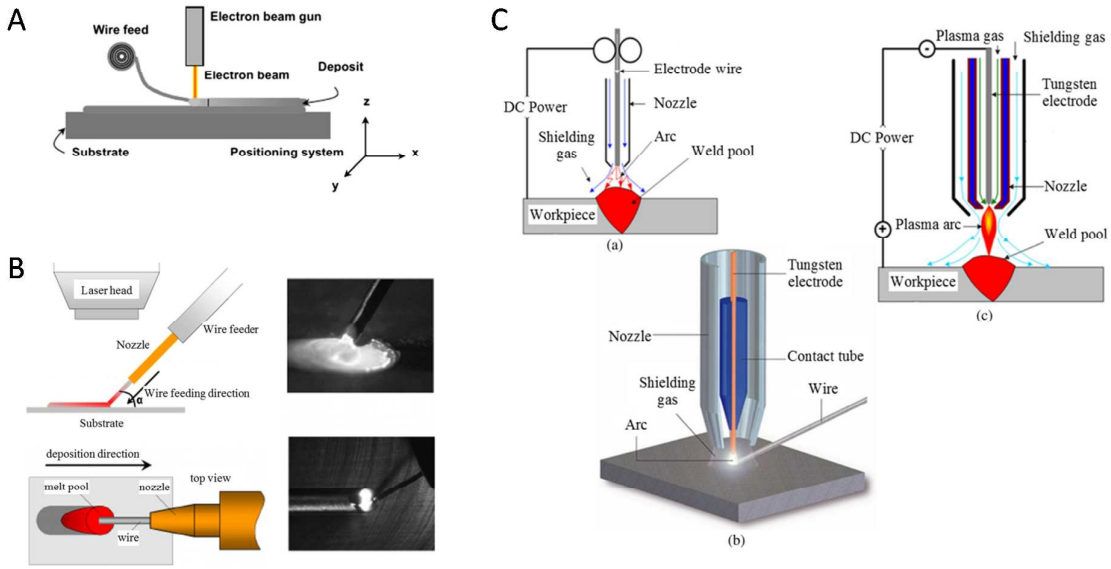

Figure 8. **A**) Schematic diagram of electron beam freeform fabrication system components. **B**) Schematic diagram of wire-laser additive manufacturing system. **C**) Schematic diagram of three possible wire-arc-welding technologies: a) gas metal arc welding (GMAW), b) gas tungsten arc welding (GTAW), and c) plasma arc welding (PAW). Adapted with permission from ref [13]. Copyright (2015) Springer.

In order to reduce the costs of metal 3D printing, an interesting approach, called selective inhibition sintering (SIS), has recently been applied with success to powder-based systems in combination with metal particles. In general, metal particle sintering (or fusing) is achieved by means of expensive laser (SLS, SLM) or electron beam (EBM) systems, which bind the particles in a layer-by-layer fashion to shape a metal object. SIS works with a contrasting mechanism by spreading a layer-by-layer sequence of a sintering inhibitor over the metal particle bed. Once the layer build is completed, the entire particle block is sintered using a high-temperature oven binding all the particles except those sprayed with the inhibitor, which are then easily removed.[18,19] In this way, the sintering process is performed only once and employs a much cheaper system (oven) than those employing lasers, etc. This method can significantly reduce the price for metal 3D printers and facilitates a more conventional distribution of these machines.

Very recently, a groundbreaking 3D-printing technology has been introduced, achieving from 25 to 100 times faster printing processes compared to the advanced SLA or polyjet machines currently available. This technology is called CLIP, which stands for "continuous liquid interface production" (or printing).[20-22] The innovative approach relies on the use of an oxygen-permeable, transparent window at the bottom of a UV-curable resin container that creates a sort of "dead zone" where the dissolved oxygen inhibits polymerization. Immediately above this thin zone, polymerization can occur, dictated by the continuous projection of UV images from below the resin bath, with the object literally being pulled out as the solidified parts are formed (Figure 9). This process enables continuous formation of a solid-liquid interface and significantly accelerates the production process because it does not rely on the step-by-step layer formation found in a typical 3D-printing process.

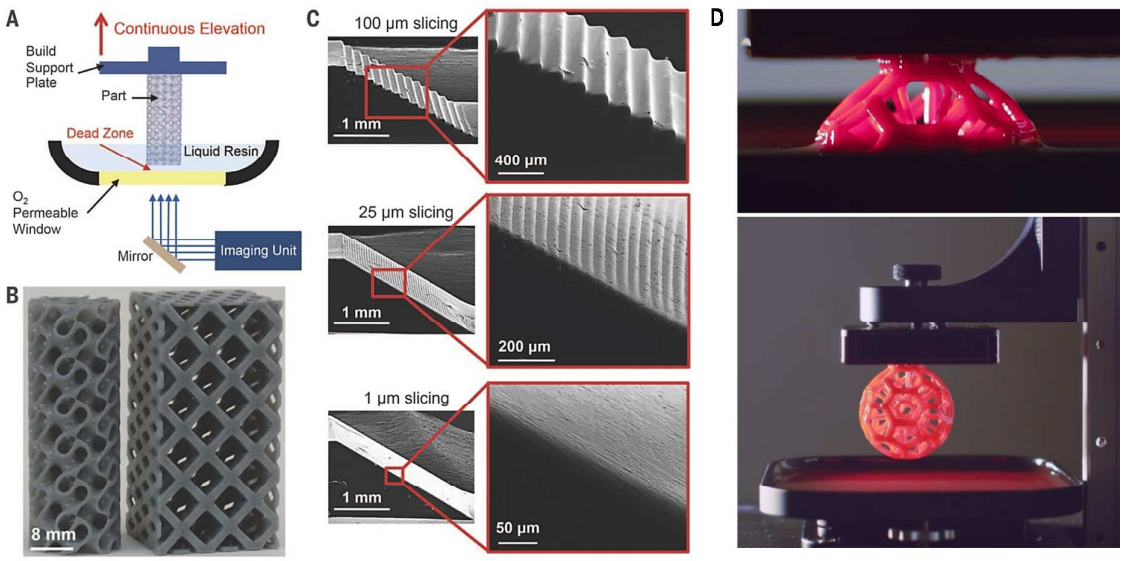

Figure 9. **A**) Schematic diagram of CLIP printer where the part (gyroid) is produced continuously by simultaneously elevating the build support plate while changing the 2D cross-sectional UV images from the imaging unit. The oxygen-permeable window creates a dead zone (persistent liquid interface) between the elevating part and the window. **B**) Resulting parts via CLIP, a gyroid (left) and an argyle (right), were elevated at print speeds of 500 mm/hour. **C**) Ramp test patterns produced at the same print speed regardless of 3D model slicing thickness (100 µm, 25 µm, and 1 µm). **D**) Images taken during the printing process. Adapted with permission from ref [22]. Copyright (2015) American Association for the Advancement of Science.

Extraordinary progress has been made to improve the spatial resolution of printing systems. Recently, a technology known as direct laser writing (DLW) has been making enormous progress in developing the fabrication of millimeter-size structures with sub-100 nm spatial resolution. This technique is based on multiphoton polymerization (MPP) by means of an ultrafast (femtosecond) laser,[23] which is tightly focused inside the volume of a transparent material causing it to polymerize locally. By moving the beam according to a CAD design, a micro-sized model can be fabricated. MPP was demonstrated during the late 1990s. Today, the most promising method is based on two-photon absorption and consequent polymerization (2PP). For this technology to achieve submicrometer resolution, it is of

fundamental importance to employ highly accurate positioning systems that allow precise scanning of the laser beam over a fixed stage or precise movement of the substrate stage coupled with a fixed position laser. Significant improvements have been achieved by using piezoelectric actuators to move the stage or galvanometric mirrors to scan the laser.[24] By using this technology, extremely detailed structures can be produced (Figure 10).

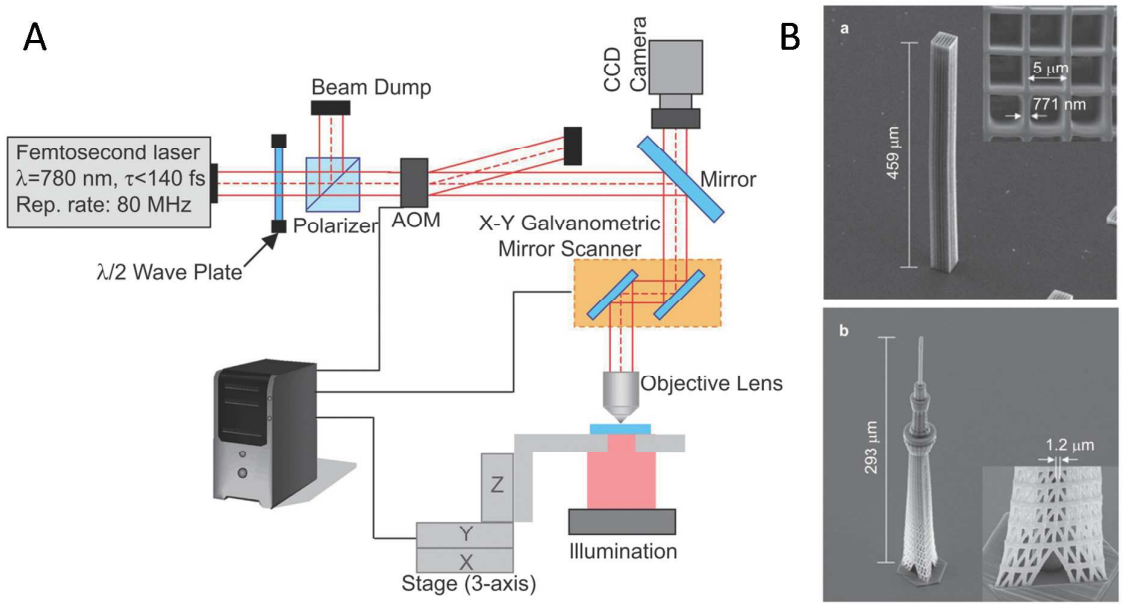

Figure 10. **A**) Typical experimental setup consisting of a light source, beam and sample movement components, beam control and focusing optics, and a vision system. **B**) SEM images of (a) 6×6 grid structure and (b) a "Tokyo Skytree" miniature. Both structures were fabricated by 2PP with 100× high-magnification microscope objective. Reprinted with permission from ref [24]. Copyright (2013) Nature Publishing Group.

Table 1. Summary of 3D-printing methods.

3D-printing process	Technique	Materials	Advantages	Limitations
Photopolymerization	Stereolithography (SLA)	Photopolymers	Simple	Single material
	Material jetting	Photopolymers	Multimaterial structures	High cost
	Continuous liquid interface printing (CLIP)	UV-curable resins	High speed	Single material
	Two-photon polymerization (2PP)	UV-curable resins	Sub-100 nm resolution	Low yield of production
Extrusion	Fused deposition modeling (FDM)	Thermoplastics (ABS, PLA, PC, PA, etc.); glass (new); metal (new)	Simple, low cost (for thermoplastic materials)	Complex; high cost (for glass and metal)
	Robocasting (DIW)	Plastics, ceramic, food, living cells, composites	Versatile	Requires post-processing; low resolution
Powder based	Selective laser sintering (SLS)	Thermoplastics, metals	No need for support material	Limited mechanical properties of object; high cost
	Selective laser melting (SLM)	Metals	No need for support material	High cost
	Electron beam melting (EBM)	Metals	No need for support material	High cost
	Binder jetting	Any material in particulate form	No need for support material; versatile; lower cost than laser-based methods	Limited mechanical properties
	Selective inhibition sintering (SIS)/inhibitor jetting	Metal	Sintering is performed only once, at the end of printing; lower cost than laser-based methods	Low resolution; limited mechanical properties
Lamination	Laminated object manufacturing (LOM)	Paper, metal, plastic, etc. as laminated sheets	Simple, versatile	Limited mechanical properties; some design limitations

3. 3D printing for electrochemistry

Electrochemistry can certainly benefit from the use of 3D-printing technologies because they facilitate the construction of custom-made complex measurement systems at reduced prices and with great versatility. In particular, 3D printing can be employed to produce conductive electrodes with special shapes or compositions to be used for redox and catalytic processes and/or to build liquid handling systems, such as voltammetric cells or micro-macrofluidic systems, which can then be combined with electrodes. One of the first attempts at producing conductive materials through additive manufacturing was made by Czyżewski *et al*. who used a binder jetting 3D-printing machine to fabricate a plaster-based block.[25] After the printing process, a fragile and porous structure was obtained, which required post-process impregnation with epoxy resin to harden the structure and obtain the desired mechanical properties. The authors proposed the use of a carbon nanofiber-epoxy resin mixture to harden the structure and at the same time confer electrical conductivity.[25] In a recent development, direct 3D printing of carbon-based conductive materials has been demonstrated using graphene composites. Wei *et al*. were able to prepare graphene composites with acrylonitrile-butadiene-styrene (ABS) and poly (lactic acid) (PLA), which were then successfully used with a commercial FDM printer to produce conductive 3D models (Figure 11).[26]

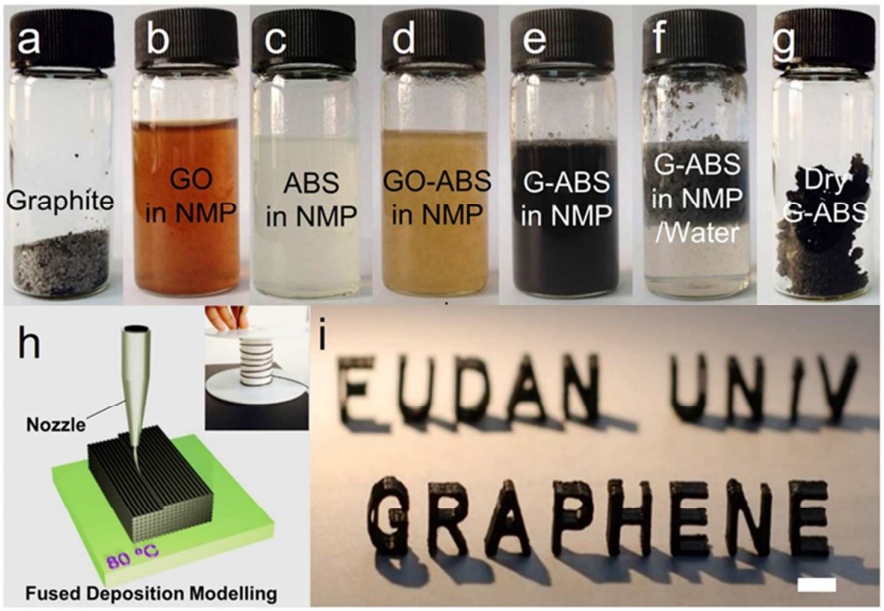

Figure 11. Composite preparation and 3D printing. a) Picture of graphite flakes. b, c) Dispersions of GO and ABS in NMP solvent. d, e) Pictures showing a homogeneous mixture of GO-ABS in NMP before and after chemical reduction by hydrazine hydrate at 95 °C for 1 h. Brownish GO-ABS turned into black G-ABS suspension during chemical reduction. f) G-ABS coagulations obtained after isolation (e) with water. g) G-ABS composite powder after washing and drying. h) Schematic illustration of fused deposition modelling 3D printing process. Inset is the graphene-based filament winding on a roller. The filament was deposited through a nozzle onto a heated building plate, whose temperature was set at 80 °C. i) A typical 3D printed model using 3.8 wt. % G-ABS composite filament, scale bar: 1 cm. Reprinted with permission from ref [26]. Copyright (2015) Nature Publishing Group.

In another work, Zhu *et al*. prepared graphene oxide inks with suitable rheological properties to be printed by the direct ink writing method (robocasting). 3D graphene-based aerogel structures were produced with outstanding mechanical and electrical properties (Figure 12).[8] The method presented in this work enables the fabrication of a broad class of 3D macroscopic graphene aerogel structures with different geometries, and could lead to new types of graphene-based electronics, energy storage devices, catalytic scaffolds, and separation devices.[8]

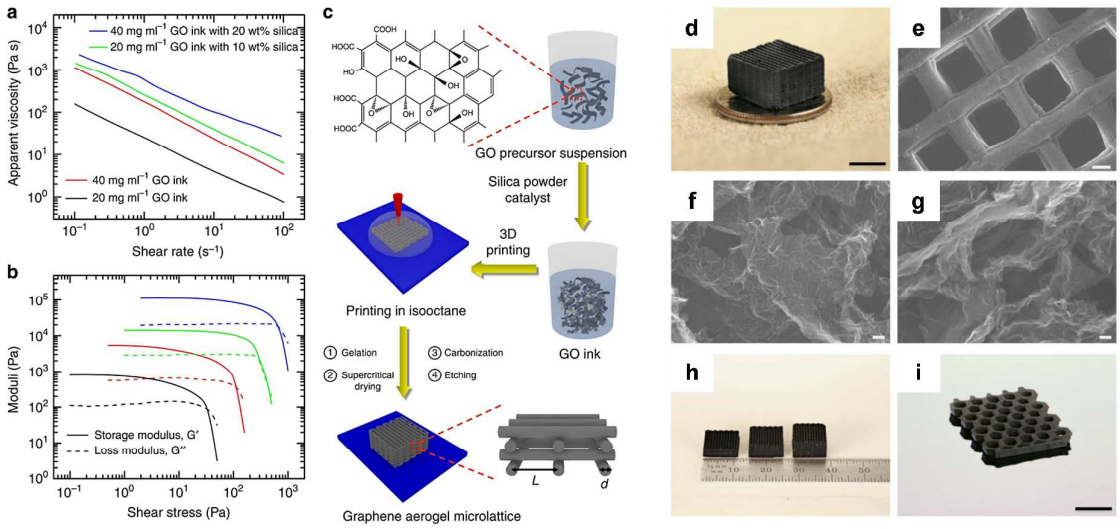

Figure 12. Fabrication strategy and rheological properties of GO ink. Log–log plots of (**a**) apparent viscosity as a function of shear rate and (**b**) storage and loss modulus as a function of shear stress of GO inks with and without silica fillers. (**c**) Schematic diagram of the fabrication process. Following the arrows: fumed silica powders and catalyst (i.e., $(NH_4)_2CO_3$ or R–F solution) were added into as-prepared aqueous GO suspensions. After mixing, a homogeneous GO ink with designed rheological properties was obtained. The GO ink was extruded through a micronozzle immersed in isooctane to prevent drying during printing. The printed microlattice structure was supercritically dried to remove the liquid. Then, the structure was heated to 1050 ^{o}C under N_2 for carbonization. Finally, the silica filler was etched using HF acid. The in-plane center-to-center rod spacing is defined as L, and the filament diameter is defined as d. (**d**) Optical image of a 3D printed graphene aerogel microlattice. SEM images of (**e**) a 3D printed graphene aerogel microlattice, (**f**) graphene aerogel without R–F after etching, and (**g**) graphene aerogel with 4 wt% R–F after etching. Optical image of (**h**) 3D printed graphene aerogel microlattices with varying thicknesses and (**i**) 3D printed graphene aerogel honeycomb. Scale bars: 5 mm (d), 200 μm (e), 100 nm (f, g), 1 cm (i). Reprinted with permission from ref [8]. Copyright (2015) Nature Publishing Group.

One of the first applications of 3D printing for electrochemistry was demonstrated by Snowden *et al*. in 2010, designing a versatile flow cell which can easily accommodate

different types of electrodes for specific electrochemical experiments. They employed SLA deposition technology for the printing process and used ferrocenylmethyl trimethylammonium ($FcTMA^+$) hexaflorophosphate redox probe in 0.1 M KNO_3 supporting electrolyte (Figure 13).[27] In this work, the authors performed a series of experiments aiming to investigate the electrochemical signals generated by the redox probe in relation to different volume flow rates and comparing the results with numerical simulations.

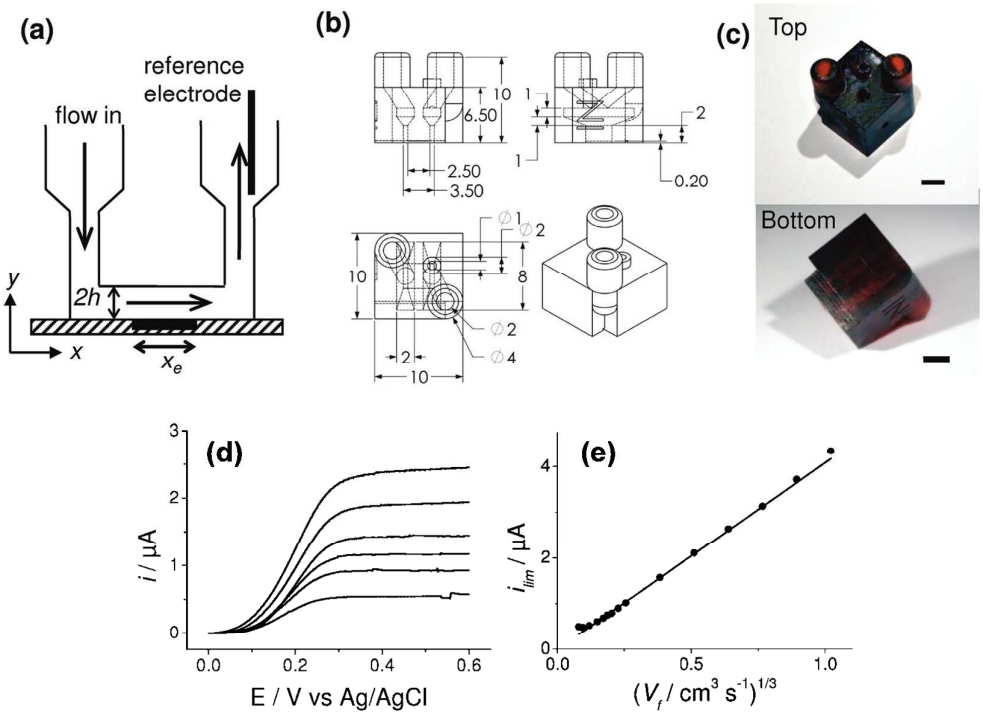

Figure 13. (**a**) Schematic diagram of the channel electrode geometry comprising a working electrode of length x_e , a channel of height 2h, and width of w (perpendicular in direction to both x_e and h), (**b**) design and key dimensions (millimeters) of the one-piece flow cell, and (**c**) photographs of a finished MSL-produced flow cell. Scale bars: 3 mm. (**d**) Typical LSVs for the oxidation of 0.1 mM $FcTMA^+$ in 0.1 M KNO_3 at Au band channel electrode at 10 mV s^{-1} at V_f values of 0.03, 0.2, 0.5, 1.0, 3.4, and 8.0 mL min^{-1}. (**e**) Comparison of experimentally obtained i_{lim} (●) to the Levich equation (solid black line), over V_f range of 0.03 - 64 mL min^{-1}. Reprinted with permission from ref [27]. Copyright (2010) American Chemical Society.

More recently, a complete electrochemical flow cell has been fabricated by additive manufacturing using FDM printing and then tested for mass transport and electrochemical experiments. Nickel foil electrodes were integrated and assembled in the printed cell device in addition to a liquid handling system.[28]

After surveying these first attempts at proof-of-concept electrochemical materials and devices fabricated by additive manufacturing, we wish to review reports of employing printed devices for real-world electrochemical applications. These will be presented in the following sections and are categorized according to scope.

3.1 Sensing

3D printing based on photopolymerization has been employed to fabricate special electrodes to be used for dry measuring and recording of electroencephalograms (EEG) and electrocardiograms (ECG). The use of dry electrodes is beneficial in that it avoids the application of gels to lower the impedance between skin and electrodes and also does not require the application of problematic Ag/AgCl reference electrodes that are used for wet measurements.[29] Dry electrodes have been produced as an array of conical needles in plastic material followed by successive sputter-coating of a titanium adhesion layer and gold, which significantly reduces the impedance, enabling reliable measurements even in the presence of hair (Figure 14). The electrodes were tested in parallel with conventional gel-based systems obtaining perfectly matched recordings.[29]

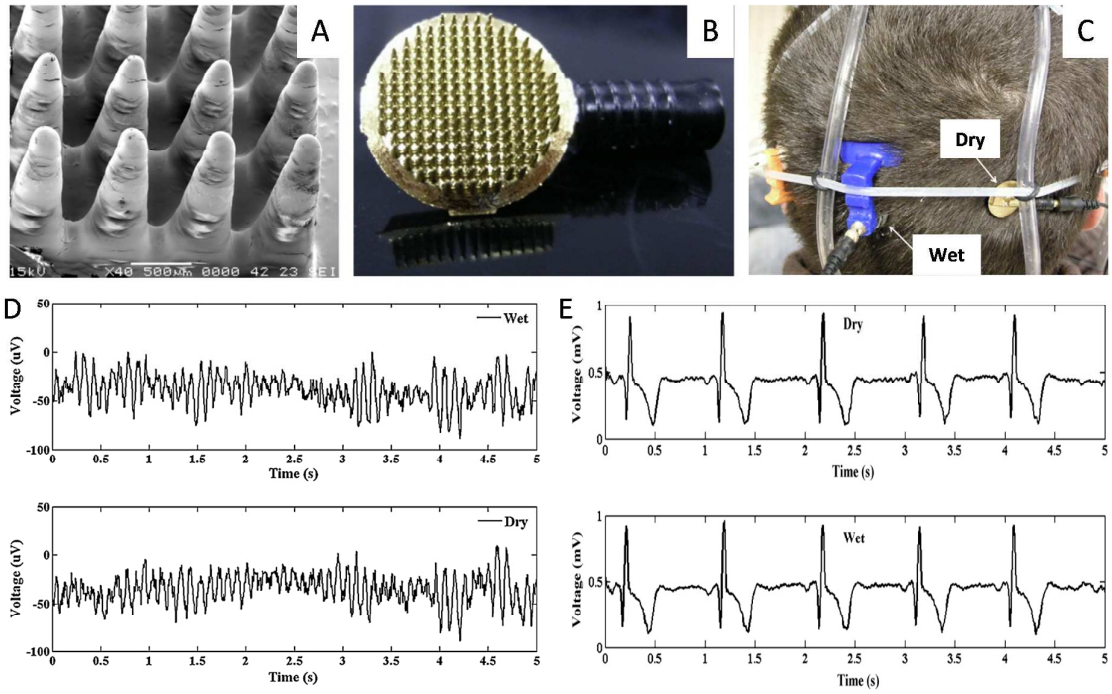

Figure 14. **A**) Partial SEM image of electrode tilted by 35°. **B**) 3D printed electrode in its final form. **C**) Dry and wet electrodes positioning for EEG measurements. **D**) Alpha waves (EEG) recorded with wet (upper) and dry (lower) electrodes. **E**) ECG recorded with dry (upper) and wet (lower) electrodes. Reprinted with permission from ref [29]. Copyright (2012) Elsevier.

A polylactic acid (PLA)-based microfluidic chip that was recently fabricated using the SLA 3D-printing method was applied for the detection of influenza virus. The chip was specifically designed to allow for the placement of electrodes for electrochemical measurements, tubing for handling liquid and, in addition, a magnet to control magnetic particles for the assay. In this work, CdS quantum dots were used as detecting labels.[30] A similar approach was used by Erkal *et al*. who designed and fabricated a versatile microfluidic chip with treated ports, which allowed the insertion of tubes and electrodes. For this work, they employed polyjet 3D printing using transparent acrylate-based polymer to

fabricate the chip, which was deployed for the detection of dopamine, nitric oxide, and ATP.[31] Another application for a 3D printed microchip device was recently demonstrated. In this work, a microfluidic system was integrated with commercially available microdialysis probes, allowing for continuous monitoring of tissue analytes such as lactate, glucose, etc.[32] This device could be used for testing athlete's performance during sports activities in real-time, as well as for bedside patient monitoring in hospitals.[32]

3D printing methods based on photopolymerization were recently adopted with great advantages for the fabrication of microneedle-based systems which could be used for both transdermal delivery of pharmacological agents[33] and sensing applications.[34] With regard to the sensing devices, electrochemical detection proved to be the most appropriate giving the possibility to detect several biologically relevant analytes.[35and references therein

Miller *et al*. employed micro-stereolythography to fabricate hollow microneedles in an array format for the simultaneous and selective amperometric detection of pH, glucose, and lactate.[35] More recently two-photon polymerization (2PP) was adopted to fabricate hollow microneedles which were then combined with a PMMA microfluidic chip for the transdermal potentiometric detection of K^+ (Figure 15).[36] In this work authors compared the performance of porous carbon and porous graphene as transducers materials for the ion-selective-electrode (ISE) with the former showing better electrochemical performances. This was the first demonstration of a microneedle-based ISE sensor.

A microfluidic device was recently fabricated by the FDM 3D-printing method and employed for the synthesis of Prussian blue nanoparticles as well as a sensing system for the analysis of hydrogen peroxide using integrated gold electrodes.[37]

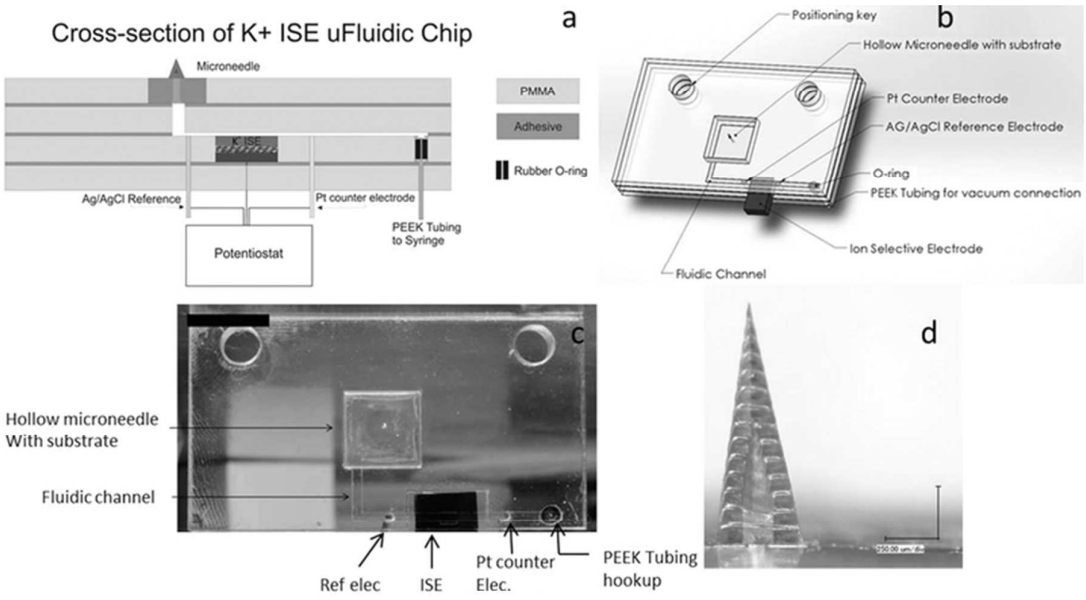

Figure 15. **a**) CorelDraw rendering of a cross-section of the K^+ ISE microfluidic chip. **b**) Solidworks drawing of K^+ ISE microfluidic chip. **c**) Image of microfluidic chip with on chip reference and counter electrodes (scale bar = 10 mm) and **d**) optical image of single hollow microneedle made with two-photon lithography (scale bar = 250 = μm). Reprinted with permission from ref [36].Copyright (2014) the Wiley-VCH.

3.2 Energy-related applications

A 3D micropatterning system was employed by Izumi *et al*. to produce three-dimensional electrodes with high aspect ratio for lithium ion batteries (LIBs). The authors prepared a $Li_4Ti_5O_{12}$ composite slurry with *N*-methylpyrrolidone (NMP) which was then printed over the aluminum current collector by a multi-nozzle dispenser.[38] By using this electrode design, the assembled battery showed high charge-discharge capacity at high rates, which can be further improved by changing the height of the electrodes and the spacing.[39] More complex architectures for anode and cathode electrodes in LIBs were recently fabricated using a robocasting method.[40, 29] $Li_4Ti_5O_{12}$ for the anode and $LiFePO_4$ for the cathode were both 3D printed with a high aspect ratio in an interdigitated electrode conformation (Figure 16). The

assembled microbattery demonstrated a high areal energy density of 9.7 J cm^{-2} at a power density of 2.7 mW cm^{-2}.[40]

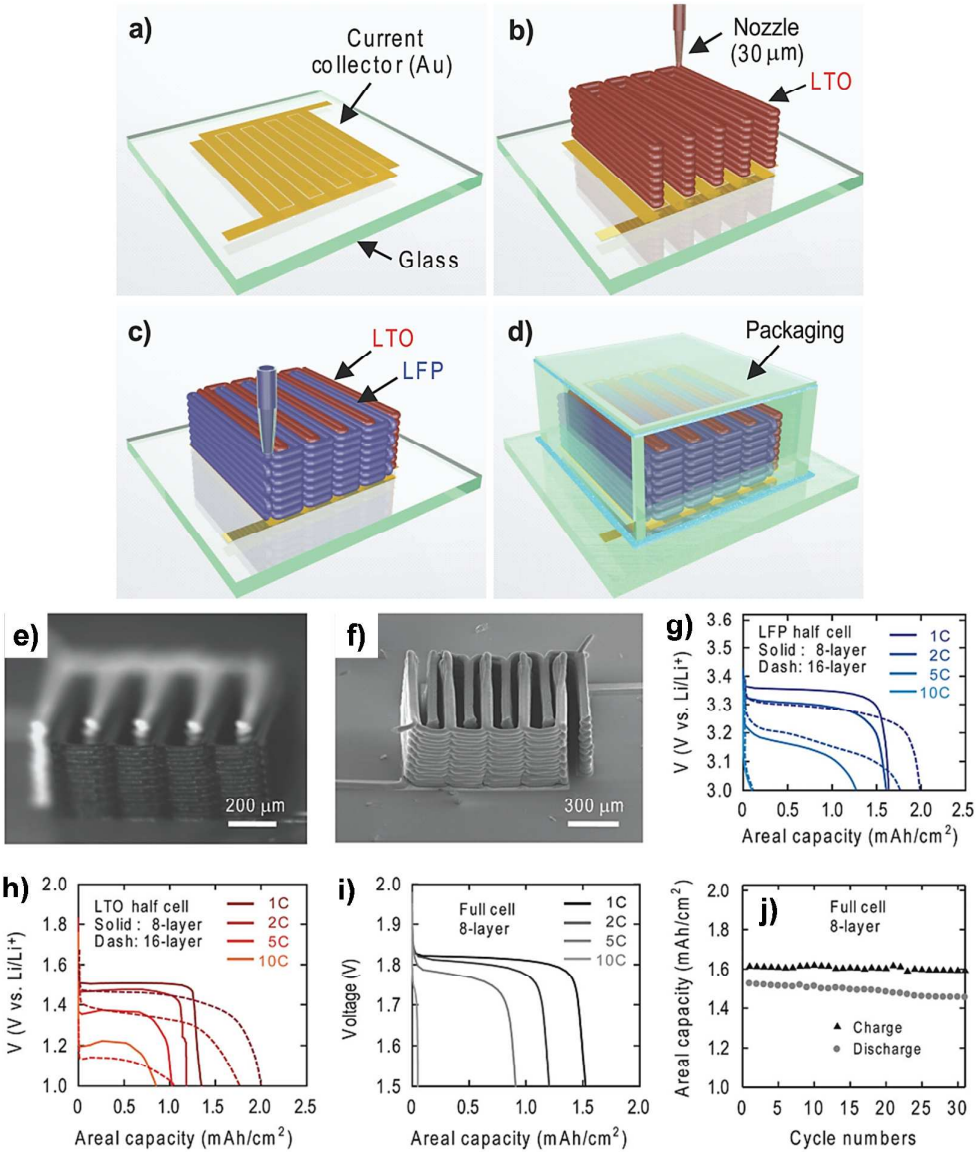

Figure 16. Schematic illustration of 3D interdigitated microbattery architectures (3D-IMA) fabricated on (a) gold current collector by printing (b) $Li_4Ti_5O_{12}$ (LTO) and (c) $LiFePO_4$ (LFP) inks through 30 µm nozzles, followed by sintering and (d) packaging. (e) Optical and (f) SEM images of printed and annealed 16-layer interdigitated LTO-LFP electrode architectures, respectively. Half-cell voltage as a function of areal capacity for (g) LFP and (h) LTO electrodes. (i) Full-cell voltage as a function of areal capacity for 8-layer interdigitated LTO-LFP electrodes. (j) Areal capacity of full cell composed of 8-layer interdigitated LTO-LFP electrodes measured as a function of number of cycles tested. Reprinted with permission from ref [40]. Copyright (2013) the Wiley-VCH.

A microextrusion 3D-printing system was employed to deposit thermally reduced graphene inks as solid electrodes for electrochemical capacitors.[41] In this work, a high surface area electrode of ~ 593 m^2 g^{-1} was obtained with good conductivity of 16 S cm^{-1} and without the need of any binder material. Measuring the capacitance at 100 and 120 Hz frequency resulted in values ranging between 3.55 and 1.76 mF cm^{-2}. A different approach was taken by Zhao *et al*. who employed selective laser melting (SLM) technology to fabricate interdigitated metal electrodes for the assembly of a supercapacitor. In this work, SLM was used to fabricate titanium electrodes with a predefined CAD design, which were then electrochemically coated with polypyrrole (PPy) as electroactive material. Using poly(vinyl alcohol) (PVA)–H_3PO_4 polymer electrolyte, the solid-state pseudo-capacitor demonstrated a volumetric capacitance of 2.4 F cm^{-3}, an energy density of 213.5 Wh m^{-3} at a current density of 3.74 mA cm^{-3}, and a power density of 15.0 kW m^{-3} at 37.4 mA cm^{-3}.[42] In our group, we employed an SLM printing machine to fabricate a series of helical-shaped stainless steel electrodes to be applied for different electrochemical applications. After controlled electrodeposition of IrO_2 thin films, the electrodes were tested for capacitive behavior in alkaline solution, for catalytic properties towards the oxygen evolution reaction, and also as a potentiometric pH sensor demonstrating excellent electrochemical properties (Figure 17).[43]

Chisholm *et al*. recently demonstrated the use of 3D printing to fabricate a polypropylene-based proton exchange membrane (PEM) water electrolyzer resulting in a significant reduction in cost and weight. This technology enables the design and fabrication of optimized flow geometries, which can facilitate the production and storage of hydrogen.[44]

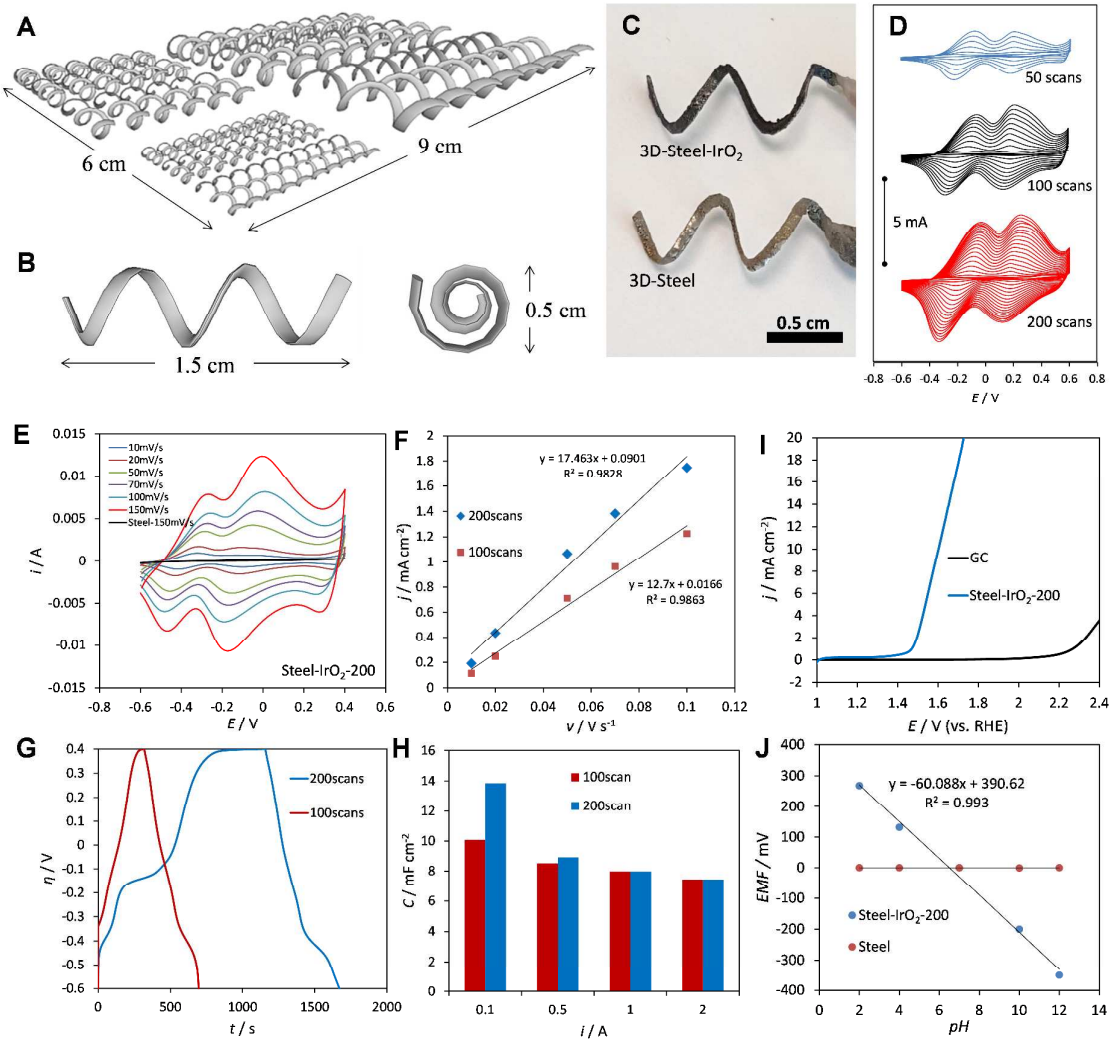

Figure 17. **A**) Schematic diagram of the electrode design used to print helical-shaped stainless steel electrodes. **B**) Dimension of electrodes employed in this work for electrochemical testing. **C**) Photograph of steel electrode as-printed and after deposition of IrO_2 film (200 scans). **D**) Cyclic voltammograms recorded for IrO_2 deposition with three different steel electrodes (same size) after 50, 100, and 200 potential scans. **E**) Cyclic voltammograms recorded for steel-IrO_2 electrode in 1 M KOH at different scan rates. **F**) Plots of current density (taken at -0.1 V) versus scan rate for steel-IrO_2 electrodes prepared with 100 (red) and 200 (blue) CV scan deposition. **G**) Charge/discharge curves for steel-IrO_2 electrodes applying 0.1 mA current. **H**) Specific capacitance for steel-IrO_2 electrodes at different applied currents, calculated from discharge curve. **I**) Polarization curve measured in 1 M KOH with steel-IrO_2 (blue) and glassy carbon (GC, black) electrodes. Current density is calculated considering the geometrical surface area of the electrodes. Scan rate: 5 mV/s. **J**) Potentiometric response (open circuit potential, OCP) of steel-IrO_2 (blue) and uncoated steel (red) electrodes at various pH values. Reprinted with permission from ref [43]. Copyright (2016) the Wiley-VCH.

3.3 Synthetic processes and electrosynthesis

The use of 3D printing to fabricate electrochemistry-based synthetic reactors is at its nascent stage. It is envisioned that the widespread expansion of this rapid prototyping technology to fabricate custom-made chemical reactors integrated with electrochemical systems will enable fast and cost-effective synthesis. 3D printed reactionware and fluidic systems for organic synthesis have already been demonstrated, showing promise of facilitating the dissemination of sophisticated synthetic chemistry hardware to less equipped labs.[45-49] Different items of miniaturized millifluidic and microfluidic reactionware equipments have been fabricated in an effortless fashion with inexpensive material using 3D printing by Kitson *et al*. (Figure 18A).[46] In this work, using different fluidic configurations (Figure 18B), the usefulness of such devices has been demonstrated for both organic and inorganic reactions as well as for the synthesis of gold nanoparticles. For example, configuration R1 was chosen for imine formation and reduction, as illustrated in Figure 18D. As depicted in Figure 18C, the reactor can be connected to a pumping system coupled to IR and/or UV-Vis analyzers (depending on the reaction).[46] In another work, self-contained chemical reactors have been 3D printed using polypropylene, where the reagents, catalysts, and starting materials were incorporated within the reactionware itself. Without the use of pumping systems and only by exploiting gravity as the sole driving force, the mixing of reagents and collection of the products were accomplished. The authors demonstrated applicability of the device by carrying out a three-step reaction: (i) Diels – Alder cyclization, a widely used C–C bond-forming reaction, followed by (ii) the formation of an imine, and finally (iii) hydrogenation of the imine to the corresponding secondary amine.[49]

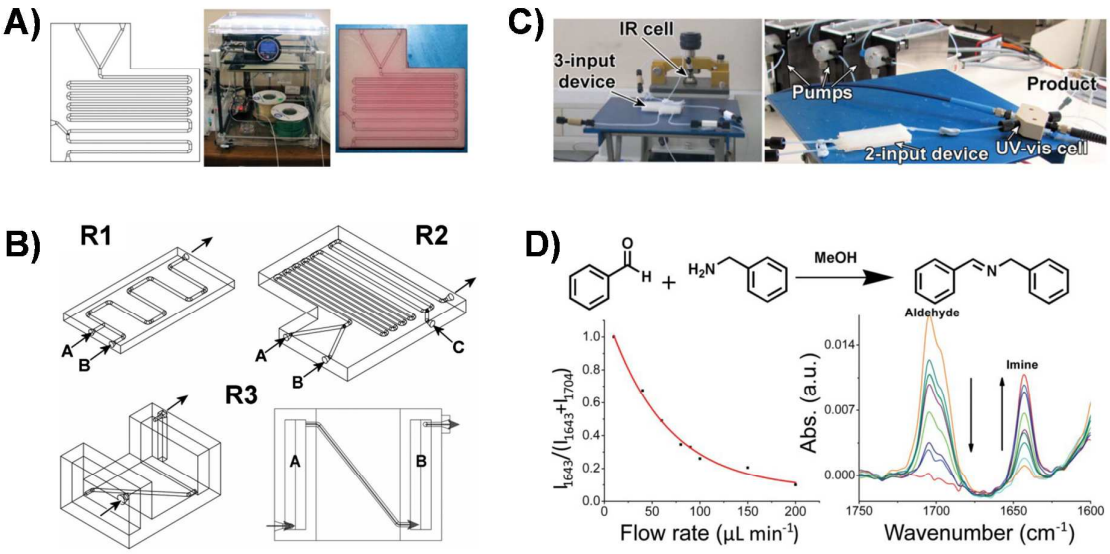

Figure 18. **A**) (Left) Schematic drawing of design of one of the reactors used in this study. (Center) 3DTouch™ 3D printer used in fabrication of the micro- and millireactors. (Right) Device printed from drawing shown on the left. The channels in the device have been filled with a methanol solution of Rhodamine B dye to render them visible. The dye can be completely removed by subsequent washing. **B**) CAD drawings of each of the three devices: (top left) R1, Two-inlet device; (top right) R2, Three-inlet device; (below) R3, One-inlet device with two "silos", one filled with sodium molybdate (A) and the other filled with hydrazine dihydrochloride (B), both as solids. An oblique and aerial view are provided. The arrows indicate the various inlets and outlets. **C**) Actual setup of the devices, with three inlets each connected to a pump, and the in-line ATR-IR and/or UV-Vis flow-cells connected to the outlet. **D**) Flow synthesis of imine derived from benzaldehyde and benzylamine, as characterized by in-line ATR-IR spectroscopy. Adapted with permission from ref [46]. Copyright (2012) Royal Sociey of Chemistry.

Considering the possibility of electrosynthesis in a 3D printed reaction vessel, one of the first examples was recently demonstrated by the Cronin group.[50] In their work, a robocasting 3D-printing system was employed to fabricate an acetylsilicone polymer-based reactor (Figure 19A, D), which was then integrated with commercially available electrodes to trigger and follow the redox conversion of phosphomolybdic acid (PMA) to polyoxomolybdates accompanied by a color change from yellow to blue (Figure 19E, F). Subsequently, the authors also demonstrated the possibility of 3D printing a full electrochemical synthetic cell coupled with the electrodes, which were obtained by mixing silicone polymer with conductive carbon black powder. Once the electrodes were connected to the potentiostat, the reaction occurred with similar efficiency, comparable to commercial electrodes (Figure 19H-J).

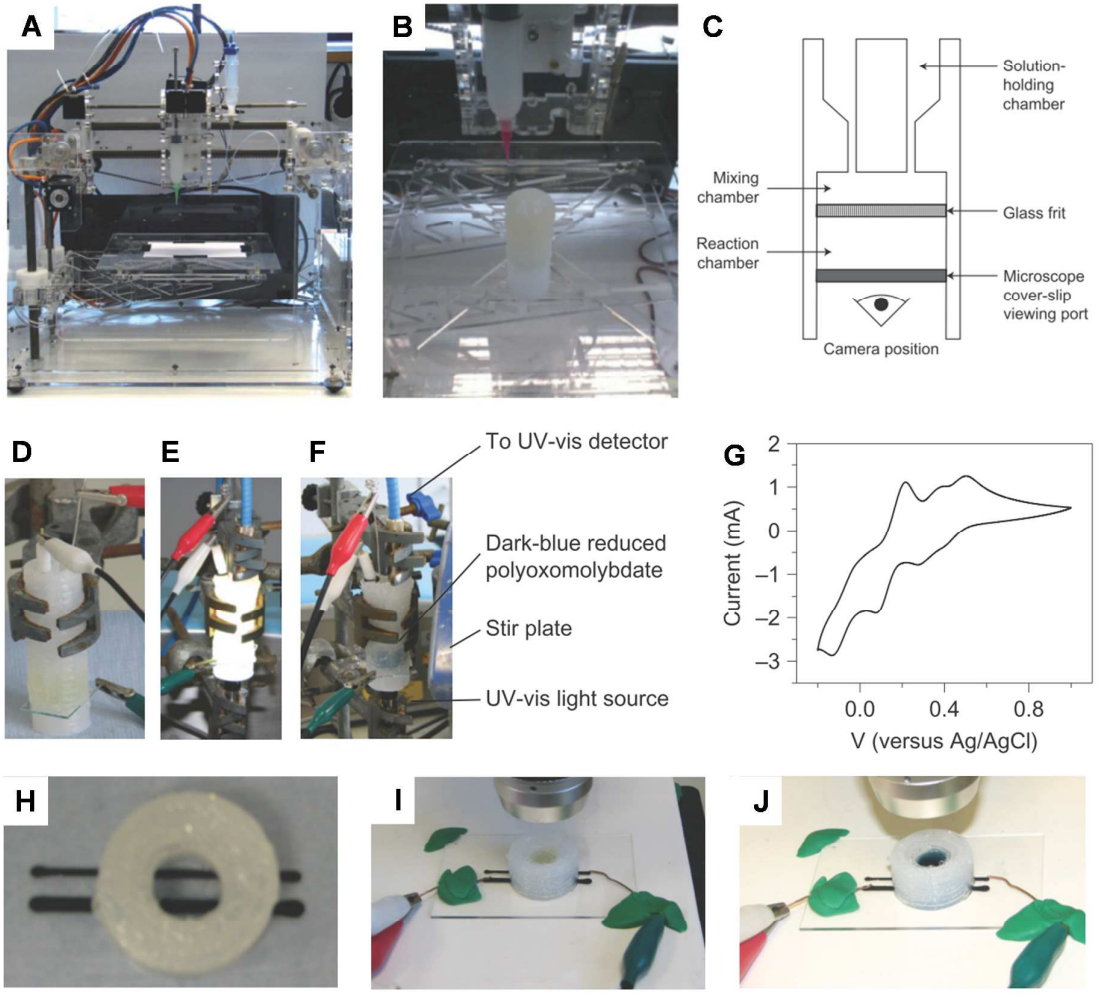

Figure 19. **A**) Fab@Home Version 0.24 RC6 freeform fabricator viewed from the front, with a single syringe of acetoxysilicone polymer loaded in the printing head. **B**) Fabricator printing one of the devices used in this work. **C**) Schematic diagram of the as-printed multipurpose reactionware used for the various syntheses, which shows the key features of the design. **D**) Reactionware as a cell for electrochemistry in a three-electrode configuration. **E, F**) Reactionware used for spectroelectrochemistry. **G**) Cyclic voltammetry, as recorded using the setup shown in (D–F), for PMA (5 mM in 0.1 M H_2SO_4) at a scan rate of 0.1 V s^{-1}. **H**) 3D printed electrochemical cell and electrodes used for in situ spectroscopies showing the two conductive electrodes based on carbon black. The working electrode (upper line) had an area exposed to the reaction medium of approximately 0.8 × 0.1 cm^2 and the reference/counter electrode rail (lower line) had an exposed area of 1.0 × 0.2 cm^2. **I**) Connected cell filled with 1 ml of 5 mM PMA in 0.1 M H_2SO_4 before electrochemical reduction. **J**) Same cell after reduction at -2.5 V for 4,500 seconds. Reprinted with permission from ref [50]. Copyright (2012) Nature Publishing Group.

4. Conclusion and future perspectives

Additive manufacturing, more commonly known as 3D printing, has become more widespread thanks to the introduction of cheaper and simpler printing machines. This technology is increasingly being considered for adoption by entities such as industry, research institutions, and laboratories, and has even reached single individuals. Organizations or people will be able to design and fabricate on-the-spot, wide-ranging objects and devices with exciting possibilities of rapid prototyping. At present, there is a wide range of different technologies in the market and, more importantly, different materials that can be used in the fabrication process. Numerous fields can benefit or are already benefiting from its use. Areas in arts and design, mechanical engineering, medicine, and also the core sciences of physics, chemistry, and materials science are increasingly taking into consideration the enormous potential of rapid prototyping through 3D printing. Electrochemistry will certainly benefit from the fabrication of such novel devices through rapid prototyping, with improved performance and at reduced cost. Due to the ease of testing new concepts and building prototypes, new opportunities for electrochemical applications in sensing, energy-related applications, and electrochemistry-assisted syntheses are now being increasingly explored through 3D printing.

Acknowledgments

We acknowledge a Tier 2 grant (MOE2013-T2-1-056; ARC 35/13) from the Ministry of Education, Singapore.

Biographies

Dr. Adriano Ambrosi *received his PhD degree from Dublin City University, Ireland in 2007. As postdoctoral researcher he firstly worked for two years at ICN (Spain), and then, in 2009, at NIMS (Japan). In 2010 he joined the research group of Prof. Martin Pumera at Nanyang Technological University (Singapore) where he currently works as Senior Research Fellow. His research interests include the application of nanomaterials to electrochemical biosensors, synthesis and fundamental electrochemical studies of graphene and other 2D materials for biosensing and energy storage devices, 3D-printing, and synthetic nanomotors.*

Prof. Martin Pumera *is a tenured faculty member at Nanyang Technological University, Singapore since 2010. He received his PhD at Charles University, Czech Republic, in 2001. After two postdoctoral stays (in the USA, Spain), he joined the National Institute for Materials Science, Japan, in 2006 for a tenure-track arrangement and stayed there until Spring 2008 when he accepted a tenured position at NIMS. In 2009, Prof. Pumera received a ERC-StG award. Prof. Pumera has broad interests in nanomaterials and microsystems, in the specific areas of electrochemistry and synthetic chemistry of carbon nanomaterials, nanotoxicity, micro and nanomachines and 3D printing. He is associate editor of PCCP, member of Editorial board of Chem. Eur. J., Electrochem. Commun., Electrophoresis, Electroanalysis, The Chemical Records, ChemElectroChem and eight other journals. He has published over 400 articles, which received over 14000 citations (h-index of 56).*

Notes and References

1 A. Gebhardt, *Understanding additive manufacturing: rapid prototyping, rapid tooling, rapid manufacturing*, Munich; Cincinnati: Hanser Publishers, 2012.
2 J. P. Davim, *Machining: Fundamentals and Recent Advances*, London: Springer-Verlag, 2008.
3 C. Barnatt, *3D printing: the next industrial revolution*, 2013.
4 H. Kodama, *Rev. Sci. Instrum.*, 1981, **52**, 1770.
5 C. W. Hull, Patents, US 4575330 A, 1986.
6 S. S. Crump, Patents, US 5121329 A, 1992.
7 U. G. K. Wegst, H. Bai, E. Saiz, A. P. Tomsia, and R. O. Ritchie, *Nat. Mater.*, 2015, **14**, 23.
8 C. Zhu, T. Y.-J. Han, E. B. Duoss, A. M. Golobic, J. D. Kuntz, C. M. Spadaccini, and M. A. Worsley, *Nat. Commun.*, 2015, **6**.
9 L. E. Murr, S. M. Gaytan, D. A. Ramirez, E. Martinez, J. Hernandez, K. N. Amato, P. W. Shindo, F. R. Medina, and R. B. Wicker, *J. Mater. Sci. Technol.*, 2012, **28**, 1-14.
10 L. E. Murr, E. Martinez, K. N. Amato, S. M. Gaytan, J. Hernandez, D. A. Ramirez, P. W. Shindo, F. Medina, and R. B. Wicker, *J. Mater. Res. Technol.*, 2012, **1**, 42-54.
11 M. Feygin, A. Shkolnik, M. N. Diamond, and E. Dvorskiy, Patents, US 5730817 A, 1998.
12 J. Klein, M. Stern, G. Franchin, M. Kayser, C. Inamura, S. Dave, J. C. Weaver, P. Houk, P. Colombo, M. Yang, and N. Oxman, *3D Printing and Additive Manufacturing*, 2015, **2**, 92.
13 D. Ding, Z. Pan, D. Cuiuri, and H. Li, *Int. J. Adv. Man. Technol.*, 2015, **81**, 465.
14 K. M. B. Taminger and R. A. Hafley, (2003) Electron beam freeform fabrication: a rapid metal deposition process. In: Proceedings of third annual automotive composites conference, Society of Plastics Engineers, Troy, MI; 9 – 10.
15 A. Heralic (2012) Monitoring and control of robotized laser metal-wire deposition. Doctoral thesis, Chalmers University of Technology.
16 J. Ding, P. Colegrove, J. Mehnen, S. Ganguly, P. M. Sequeira Almeida, F. Wang, and S. Williams, *Comput. Mater. Sci.*, 2011, **50**, 3315.
17 F. Martina, J. Mehnen, S. W. Williams, P. Colegrove, and F. Wang, *J. Mater. Process. Technol.*, 2012, **212**, 1377.
18 B. Khoshnevis, Patents, EP 1534461 B1, 2010.
19 B. Khoshnevis, M. Yoozbashizadeh, and Y. Chen, *Rapid Prototyping J.*, 2012, **18**, 144.
20 J. M. Desimone, A. Ermoshkin, N. Ermoshkin, and E. T. Samulski, Patents, WO 2014126837 A2, 2014.
21 J. M. Desimone, A. Ermoshkin, N. Ermoshkin, and E. T. Samulski, Patents, WO 2014126834 A2, 2014.
22 J. R. Tumbleston, D. Shirvanyants, N. Ermoshkin, R. Janusziewicz, A. R. Johnson, D. Kelly, K. Chen, R. Pinschmidt, J. P. Rolland, A. Ermoshkin, E. T. Samulski, and J. M. DeSimone, *Science*, 2015, **347**, 1349.
23 M. Malinauskas, M. Farsari, A. Piskarskas, and S. Juodkazis, *Physics Rep.*, 2013, **533**, 1.
24 K. Obata, A. El-Tamer, L. Koch, U. Hinze, and B. N. Chichkov, *Light Sci. Appl.*, 2013, **2**, e116.
25 J. Czyżewski, P. Burzyński, K. Gaweł, and J. Meisner, *J. Mat. Proc. Technol.*, 2009, **209**, 5281.

26 X. Wei, D. Li, W. Jiang, Z. Gu, X. Wang, Z. Zhang, and Z. Sun, *Sci. Rep.*, 2015, **5**, 11181.
27 M. E. Snowden, P. H. King, J. A. Covington, J. V. Macpherson, and P. R. Unwin, *Anal. Chem.*, 2010, **82**, 3124.
28 C. Ponce De Leon, W. Hussey, F. Frazao, D. Jones, E. Ruggeri, S. Tzortzatos, R. Mckerracher, R. G. A. Wills, S. Yang, and F. Walsh, *Chem. Eng. Trans.*, 2014, **41**, 1.
29 P. Salvo, R. Raedt, E. Carrette, D. Schaubroeck, J. Vanfleteren, and L. Cardon, *Sens. Act. A: Physical*, 2012, **174**, 96.
30 L. Krejcova, L. Nejdl, M. A. M. Rodrigo, M. Zurek, M. Matousek, D. Hynek, O. Zitka, P. Kopel, V. Adam, and R. Kizek, *Biosens. Bioelectron.*, 2014, **54**, 421.
31 J. L. Erkal, A. Selimovic, B. C. Gross, S. Y. Lockwood, E. L. Walton, S. McNamara, R. S. Martin, and D. M. Spence, *Lab Chip*, 2014, **14**, 2023.
32 S. A. N. Gowers, V. F. Curto, C. A. Seneci, C. Wang, S. Anastasova, P. Vadgama, G.-Z. Yang, and M. G. Boutelle, *Anal. Chem.*, 2015, **87**, 7763.
33 S. D. Gittard, A. Ovsianikov, B. N. Chichkov, A. Doraiswamy and R. J. Narayan, *Expert Opin. Drug Del.*, 2010, **7**, 513.
34 P. R. Miller, R. J. Narayan and R. Polsky, *J. Mater. Chem. B*, 2016, **4**, 1379.
35 P. R. Miller, S. A. Skoog, T. L. Edwards, D. M. Lopez, D. R. Wheeler, D. C. Arango, X. Xiao, S. M. Brozik, J. Wang, R. Polsky and R. J. Narayan, *Talanta*, 2012, **88**, 739.
36 P. R. Miller, X. Xiao, I. Brener, D. B. Burckel, R. Narayan and R. Polsky, *Adv. Healthcare Mater.*, 2014, **3**, 876.
37 G. W. Bishop, J. E. Satterwhite, S. Bhakta, K. Kadimisetty, K. M. Gillette, E. Chen, and J. F. Rusling, *Anal. Chem.*, 2015, **87**, 5437.
38 A. Izumi, M. Sanada, K. Furuichi, K. Teraki, T. Matsuda, K. Hiramatsu, H. Munakata, and K. Kanamura, *Electrochim. Acta*, 2012, **79**, 218.
39 A. Izumi, M. Sanada, K. Furuichi, K. Teraki, T. Matsuda, K. Hiramatsu, H. Munakata, and K. Kanamura, *J. Power Sources*, 2014, **256**, 244.
40 K. Sun, T.-S. Wei, B. Y. Ahn, J. Y. Seo, S. J. Dillon, and J. A. Lewis, *Adv. Mater.*, 2013, **25**, 4539.
41 T. Nathan-Walleser, I.-M. Lazar, M. Fabritius, F. J. Tölle, Q. Xia, B. Bruchmann, S. S. Venkataraman, M. G. Schwab, and R. Mülhaupt, *Adv. Funct. Mater.*, 2014, **24**, 4706.
42 C. Zhao, C. Wang, R. Gorkin III, S. Beirne, K. Shu, and G. G. Wallace, *Electrochem. Commun.*, 2014, **41**, 20.
43 A. Ambrosi, J. G. S. Moo, and M. Pumera, *Adv. Funct. Mater.*, 2016, **26**, 698.
44 G. Chisholm, P. J. Kitson, N. D. Kirkaldy, L. G. Bloor, and L. Cronin, *Energy Environ. Sci.*, 2014, **7**, 3026.
45 V. Dragone, V. Sans, M. H. Rosnes, P. J. Kitson, and L. Cronin, *Beilstein J. Org. Chem.*, 2013, **9**, 951.
46 P. J. Kitson, M. H. Rosnes, V. Sans, V. Dragone, and L. Cronin, *Lab Chip*, 2012, **12**, 3267.
47 P. J. Kitson, R. J. Marshall, D. Long, R. S. Forgan, and L. Cronin, *Angew. Chem. Int. Ed.*, 2014, **53**, 12723.
48 J. S. Mathieson, M. H. Rosnes, V. Sans, P. J. Kitson, L. Cronin, *Beilstein J. Nanotechnol.* , 2013, **4**, 285.
49 P. J. Kitson, M. D. Symes, V. Dragone, and L. Cronin, *Chem. Sci.* , 2013 , **4** , 3099.
50 M. D. Symes, P. J. Kitson, J. Yan, C. J. Richmond, G. J. T. Cooper, R. W. Bowman, T. Vilbrandt, and L. Cronin, *Nat. Chem.*, 2012, **4**, 349.